Scilight

Bulletin of Computational Intelligence
https://www.sciltp.com/journals/bci

Article

Check for updates

Hybrid Artificial Neural Network Models for Predicting Flexural Strength of FRP-Reinforced Concrete Beams

Mudassir Iqbal [1,*], Muhammad Raheel [2,*] and Rahul Biswas [3]

[1] Department of Civil Engineering, University of Engineering & Technology Peshawar, Peshawar 25120, Pakistan
[2] Interdisciplinary Research Centre—Construction and Building Materials, King Fahd University of Petroleum & Minerals, Dhahran 31261, Saudi Arabia
[3] Department of Applied Mechanics, Visvesvaraya National Institute of Technology, Nagpur 440010, India
* Correspondence: mudassiriqbal29@uetpeshawar.edu.pk (M.I.): Muhammad.raheel@kfupm.edu.pk (M.R.)

How To Cite: Iqbal, M.; Raheel, M.; Biswas, R. Hybrid Artificial Neural Network Models for Predicting Flexural Strength of FRP-Reinforced Concrete Beams. *Bulletin of Computational Intelligence* **2026**, *2*(2), 196–212. https://doi.org/10.53941/bci.2026.100011

Received: 28 January 2026
Revised: 28 April 2026
Accepted: 12 May 2026
Published: 22 May 2026

Abstract: Artificial Neural Network (ANN) models rely on gradient descent algorithm which is sensitive to the values of initial weights and its occasional premature convergence to local minima. Metaheuristics are global optimization algorithms capable to capture the non-linear behavior of structural problems. The present study explores the application of novel hybrid algorithms in structural engineering by predicting the flexure strength of concrete beams incorporating fiber reinforced polymer (FRP) bars. Novel hybrid ANN based algorithms such as grey wolf optimizer (ANN-GWO), ant lion optimizer (ANN-ALO), Harris hawk optimizer (ANN-HHO), salp swarm (ANN-SSA), whale optimization (ANN-WOA) and particle swarm optimization (ANN-PSO) were trained and validated based on the experimental flexure strength of FRP concrete beams. Based on the results of eight distinct statistical indices and accuracy matrix, ANN-ALO model demonstrated the best performance across multiple evaluation metrics such as highest R^2 values of 0.9487 and 0.9482 and the lowest RMSE values of 0.0478 and 0.0539 during the training and testing phases, respectively. Furthermore, Taylor diagrams also illustrated that the ANN-ALO model achieved the highest correlation coefficient ($R > 0.94$) during both the training and testing phases. Finally, predicted to experimental (P/E) ratios were computed for both ANN-ALO model and ACI code formulations for concrete beams incorporating fiber reinforced polymer bars. Resultantly, strong agreement was observed between the flexural capacity estimates given by the ANN-ALO model as majority of the P/E ratios were within ±10% of the ACI formulations. These findings confirmed the reliability, resource conservancy and time efficiency of novel hybrid ANN-ALO algorithm to model complex non-linear problems in the field of structural engineering.

Keywords: flexural capacity; FRP, reinforced concrete; machine learning; accuracy analysis; hybrid ANN models

1. Introduction

Concrete is one of the largely used construction material around the globe known for its high compressive strength and durability. However, its tensile strength is almost always considered negligible (only one-tenth of compressive strength) in the field of structural engineering [1–5]. Engineering structures made of concrete has to endure different types of forces during its lifespan. Therefore, mild steel reinforcement is usually employed in concrete sections subjected to tensile stresses [6–10]. Nevertheless, mild steel reinforcement corrodes inside concrete with the passage of time [11–14]. The corrosion mechanism is an electrochemical reaction occurring in

the pore solution of concrete during which loss of electrons (oxidation) at anodic sites and reduction of oxygen at cathodic sites takes place. Resultantly, its volume expands due to oxidation of iron and jeopardizes the durability of reinforced concrete causing spalling and disintegrated surfaces. This ultimately leads towards frequent maintenance and repair activities [15–18].

Due to rapid population growth and ever-increasing demand for infrastructure, the demand for concrete has been greater than ever. However, the basic constituents of concrete such as fine aggregate, coarse aggregate and water are getting scarce day by day [19,20]. Due to these reasons and for infrastructures near coastal areas, these resources are obtained from sea beds. However, the procurement of fine aggregate and coarse aggregate from natural water bodies is disturbing the habitat of aquatic flora and fauna. Moreover, they contain aggressive salts which changes the pH of concrete solution. This leads towards early corrosion of mild steel reinforcement requiring pre-scheduled maintenance [21–25]. To tackle this problem, fiber reinforced polymer (FRP) bars were introduced. They have excellent corrosion resistance, high strength to weight ratio and low density which allows their easy handling during field operations [26–31]. Research studies have been undertaken to evaluate the durability of different types of FRPs such as carbon FRPs, basalt FRPs, glass FRPs and aramid FRPs in concrete under different conditions. As a result of these efforts, it was found that they are suitable for use in concrete under normal conditions however, the behavior of FRPs under harsh alkaline environments is still under investigation due to its complex electrochemical reactions, its interaction with concrete and long-term durability prospects [32–35].

A comprehensive understanding of FRP behavior and its consequent effects on the mechanical performance and durability characteristics of concrete under diverse environmental and loading conditions necessitates extensive experimental investigation and analytical assessment [36]. It is without any uncertainty that detailed experimentation requires time, energy and resources along with the understanding and persistence to get precise and unswerving results. Moreover, experimental programs are inherently costly and frequently necessitate extensive parametric trials to establish statistically reliable conclusions for individual variables, rendering the process laborious, time-intensive, and economically demanding [37–42]. Lately, Artificial intelligence (AI) algorithms have emerged and gained reputation among the research community due to their swift learning capacity to model numerous engineering problems by precisely forecasting the output(s) [37,43–48].

Numerous investigations have demonstrated the capability of AI techniques in modeling complex civil engineering phenomena. For instance, Baykasoglu et al. [49] implemented ANN and GEP models to predict the compressive strength of high-strength concrete. Expanding on AI-based modeling approaches, Topçu et al. [50] applied ANN and Adaptive Neuro-Fuzzy Inference System to evaluate the compressive strength of mortars incorporating metakaolin as a partial cement substitute. Likewise, Sarıdemir [51] employed ANN and fuzzy logic methodologies to assess the effect of metakaolin on cement mortar strength. Other efforts included the use of response surface methodology and neural network algorithm for predicting the compressive strength of green concrete incorporating marble and granite waste powder as a partial replacement to cement [52]. Resultantly, the response surface methodology provided optimized mix design for green concrete having maximum compressive strength. Additionally, various other models including multi-layer neural network [53], decision trees, radial basis function networks, gradient boosting trees [54], and extreme learning machine [55] have been successfully implemented to model concrete compressive strength considering different additives and supplementary materials. Murad et al. [56] employed GEP to predict the flexural strength of FRP-reinforced concrete beams, accounting for parameters such as depth and width of beam, compressive strength of concrete, FRP tensile reinforcement area, modulus of elasticity and ultimate tensile strength. The model achieved excellent predictive accuracy with R^2 values of 0.97 and 0.96 for training and testing, respectively. Furthermore, Marani and Nehdi [57] introduced a tabular generative adversarial network approach to generate synthetic data for training generalized machine learning models. Using a "Train on Synthesized—Test on Real" strategy, they predicted the shear capacity of FRP-reinforced concrete beams based on 8816 synthetic training data points and 304 real experimental data points. This methodology demonstrated strong predictive reliability achieving an R^2 value of 0.96 when validated against the complete experimental dataset. The study conducted by Fathy et al. [58] studied the capability of three different machine learning models viz., extreme gradient boosting, random forest and M5P for predicting the compressive strength of green concrete incorporating marble and granite waste powder under elevated temperatures. It was observed that gradient boosting model performed better than the other models with R^2 value of 0.9989 and MAE of 0.1351 MPa.

Literature review infers that most of the studies focused on the use of standalone AI models such as ANN, GEP and fuzzy logic for predicting the mechanical properties of concrete. However, these AI models have limitations such as ANN has slow convergence rates and traps in local minima, fuzzy logic requires strict rule definition while GEP is sensitive to genetic parameter tuning and produces fixed mathematical equations hence, rendering them unable to model complex non-linear problems.

This study contributes a novel comparative framework for six meta-heuristic optimizers specifically tuned for the non-linear behavior of FRP-reinforced concrete beams by exploring their parameter optimization capability. For this purpose, experimental flexure strength values of FRP reinforced concrete beams was obtained from the published literature. Novel hybrid ANN based algorithms such as grey wolf optimizer, ant lion optimizer, Harris hawk optimizer, salp swarm, whale optimization and particle swarm optimization were trained and validated to predict the flexure strength of FRP reinforced concrete beams considering several inputs such as the dimensions of beam and mechanical properties of concrete and FRP. Eight distinct statistical indices were employed to compare the performance of hybrid novel algorithms. Lastly, the performance of best performing hybrid algorithm was also compared with ACI code formulations for its ready application in design practices.

2. Research Methodology

Section 2 of the manuscript outlines the details of different soft computing models and descriptive analysis of dataset used for training and validation of these models. The research methodology has also been depicted in Figure 1.

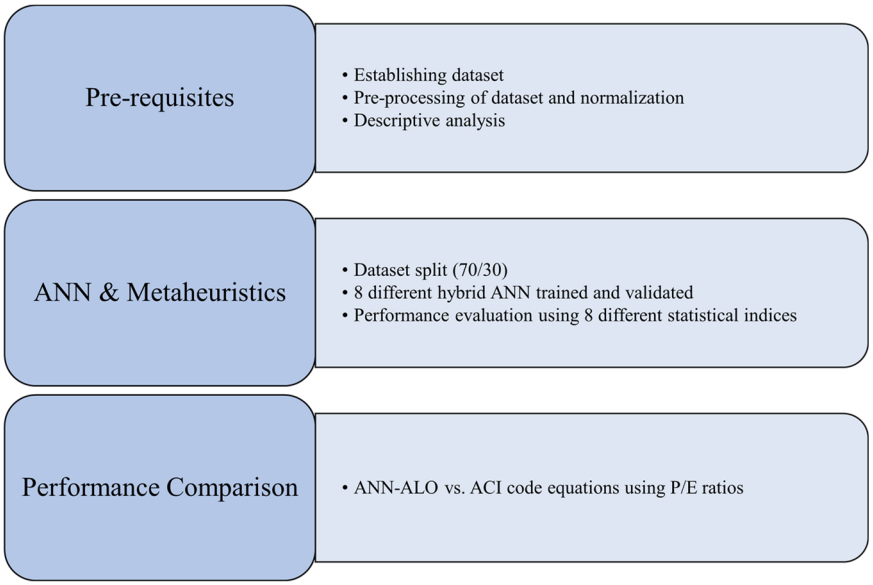

Figure 1. Methodology of proposed study.

2.1. Details of Soft Computing Models

2.1.1. ANN

The ANN algorithm is inspired by the functioning of the human brain. It simulates biological neurons to receive, process, and generate outputs. An ANN consists of interconnected neurons organized into input, hidden, and output layers, each associated with adjustable weights. During the training phase, these weights are optimized to minimize error and produce outputs that closely approximate the actual values [59,60].

2.1.2. Grey Wolf Optimization

GWO algorithm was developed in 2014 by Mirjalili et al. [61]. This algorithm has gained wide fame due to its outstanding performance and shorter convergence time. This algorithm optimizes the parameters of the model by impersonating the hunt and prey actions of the grey wolves. Recalling the hierarchical structure of grey wolves which includes the leader of the pack, known as the Alpha followed by Beta, Delta and omega. Inspired from their hunting mechanism and fulfillment of commands as per the hierarchical structure, the GWO algorithm's hierarchy is the similar and involves (a) searching, (b) encircling, (c) hunting and (d) attacking the prey.

2.1.3. Ant Lion Optimization

Inspired from the hunting mechanism of antlions, the antlion optimization (ALO) algorithm was developed which can be used in conjunction with other machine learning methods for its swift optimization. The hunt and prey mechanism of antlions involves; random ant walks, traps building, entrapping trick, catching prey and rebuilding of traps. Initially, walk and agent assortment is randomly carried out followed by the exploitation

process with the help of traps. The random walk roulette wheel strategy assists in eradicating the local optima. The originator of this model has confirmed its performance through different engineering problems such as the design of gear train, three-bar truss and cantilever beam. It was observed that the algorithm has excellent performance such as avoiding local optima, improved exploration, exploitation and convergence proficiency. The algorithm has also the ability to resolve constrained problems having diverse search space [62].

2.1.4. Harris Hawk Optimizer

The Harris Hawks Optimization algorithm was introduced by Heidari et al. [63]. It is inspired by the cooperative hunting strategies and dynamic chasing behavior of Harris hawks, which attack prey from multiple directions and adapt their tactics according to environmental conditions and escape responses. This behavior was mathematically modeled to develop an effective optimization technique. The algorithm was validated on various real-world engineering problems, demonstrating promising performance.

2.1.5. Salp Swarm Algorithm

The Salp Swarm Algorithm is inspired by the swarming behavior of salps, which form chain-like structures in deep oceans. For mathematical modeling, the population is divided into two groups: a leader positioned at the front of the chain and followers that move accordingly. Similar to other swarm-based optimization methods, the position of each search agent is represented in an n-dimensional search space [64,65], where n denotes the number of problem variables. SSA demonstrates strong exploration and exploitation capabilities, enabling it to avoid local optima and identify high-quality solutions.

2.1.6. Whale Optimization Algorithm

Humpback whales are a class of gentle and non-aggressive species. They affectionately show collaboration with each other to gain a particular output. Considering their collaborative nature and gentle interaction with each other to achieve a target, Whale Optimization Algorithm (WOA) was developed by Mirjalili and Lewis [66]. The algorithm acclimates from the bubble-net hunting tactic of the humpback whales. The designers of this algorithm have evaluated its performance using different mathematical and structural design optimization problems and observed acceptable results.

2.1.7. Particle swarm Optimization

Enthused from the working of bird flocks and schooling fish swarms, the particle swarm optimization (PSO) algorithm was presented by Eberhart and Kennedy [67]. This algorithm imitates the supportive behavior of individuals present in a population (bird flock and fish swarms). In that population, all of the individuals strive for a mutual goal which assists in its swift achievement for instance, searching locations for food and water. Considering this, the algorithm allocates specific fitness values to the individuals which moves with a particular velocity while, searching for the target. The position of each individual is repeatedly updated keeping in view their fitness values in order to reach an optimized solution.

2.2. Collection of Experimental Data & Analysis

Descriptive Analysis and Correlation

A reliable and accurate experimental database is necessary for training and testing any AI model. To model the flexure strength (FS) of concrete incorporating FRP bars using hybrid ANN models, the experimental datapoints were taken from the research study of Murad et al. [56] wherein, he predicted the FS of FRP reinforced concrete beams using GEP model (Appended as Table A1). The database is comprised of 134 datapoints with 6 distinct input parameters and one output i.e., FS. The input parameters included width of beam (b), compressive strength of concrete ($f'c$), depth of beam (d), FRP tensile reinforcement area (A_s), modulus of elasticity of FRP material (E_f) and ultimate strength of FRP material (f_u, MPa). The descriptive statistics of the dataset used for hybrid modeling are presented in Table 1 while the frequency histograms of the input variables are illustrated in Figure 2. The histograms indicate peaked distributions with relatively heavy tails, consistent with the positive kurtosis values reported in Table 1. Additionally, the positive skewness values suggest right-skewed distributions, characterized by longer tails on the higher-value side. Pearson correlation coefficients between input and output variables are presented in Figure 3.

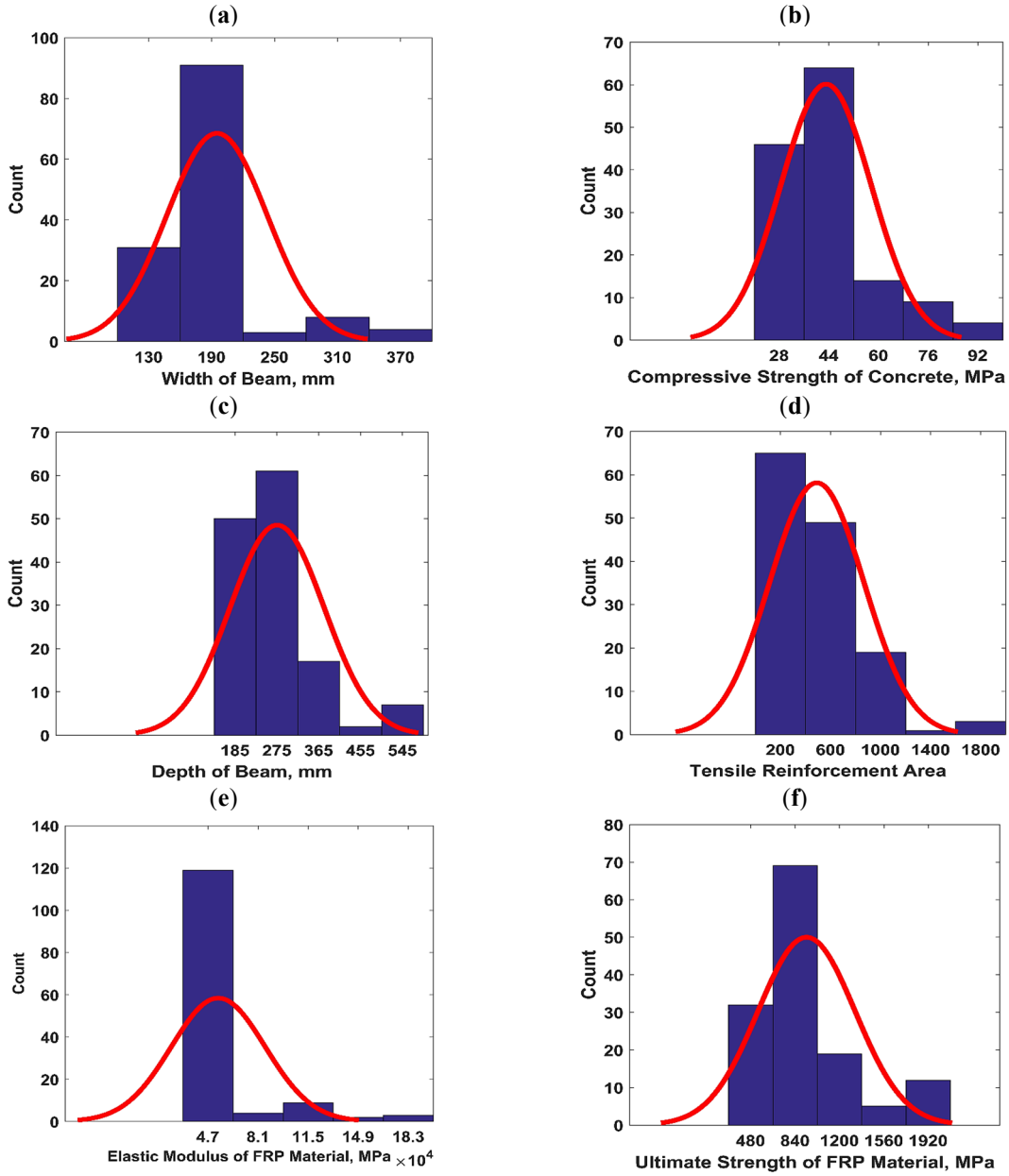

Figure 2. Frequency histograms of input parameters; (**a**) width of beam, (**b**) compressive strength of concrete, (**c**) depth of beam, (**d**) FRP tensile reinforcement area, (**e**) modulus of elasticity of FRP material and (**f**) ultimate strength of FRP.

Table 1. Descriptive details of dataset.

Statistics	b, mm	$f'c$, MPa	D, mm	A_s, mm^2	E_f, MPa	f_u, MPa
Mean	194.25	274.40	42.85	482.85	53,060	927.59
Standard error	3.91	8.56	1.20	30.75	2549.69	33.19
Standard deviation	45.26	99.12	13.84	356.00	29,514.79	384.19
Sample variance	2048.82	9825.07	191.59	126,733.21	871,122,727	147,598.15
Kurtosis	6.00	0.70	3.37	3.21	9.93	2.17
Skewness	2.02	0.88	1.61	1.46	3.09	1.71
Minimum	130.00	152.00	24.00	57.00	35,630	552
Maximum	381.00	550.00	97.00	1964.00	200,000	2069

The performance of the ANN based-hybrid models must be verified and confirmed through numerous statistical indices to have an impression about their precision and accuracy during both the Training (TR) and Testing (TS) phases, respectively. Keeping this in view, different performance indices were employed namely coefficient of determination (R^2), RMSE, variance account for (VAF), Willmott's index of agreement (WI), performance index (PI), mean absolute error (MAE), RMSE to observation's standard deviation ratio (RSR) and weighted mean

absolute percentage error (WMAPE) as they have been satisfactorily used in previous studies [49,68,69]. It is important to mention here that these indices have been calculated based on the normalized values of the input variables. Table 2 presents the ideal values and range for these different statistical indices.

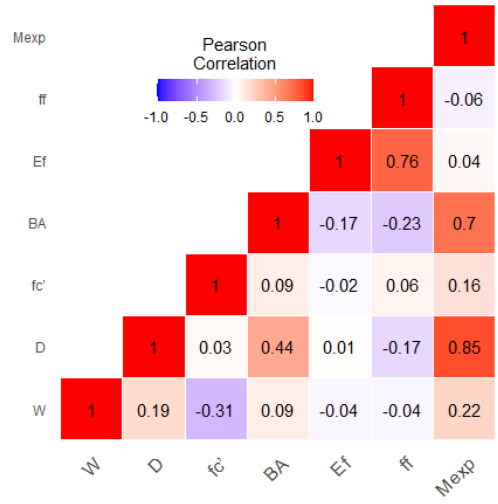

Figure 3. Pearson correlation of input and output parameters.

Table 2. Ideal values and range of different statistical indices.

Parameter	R^2	RMSE	VAF	WI	PI	MAE	RSR	WMAPE
Range	0–1	0–∞	0–100	0–1	−∞–∞	0–<∞	0–∞	0–<∞
Model value	1	0	100	1	2	0	0	0

3. Results and Discussion

3.1. Simulation of Soft Computing Models

The current study utilized 134 experimental datapoints to train and validate different ANN based hybrid algorithms considering six input parameters. The dataset was normalized using the Min-Max normalization technique during the preprocessing phase and divided into training (70%, 93 samples) and testing (30%, 41 samples) subsets. Model performance was evaluated using eight statistical metrics including correlation coefficients, variance measures and error indices. A comparative analysis of the developed models is presented in the subsequent sections and the modeling framework is illustrated in Figure 4.

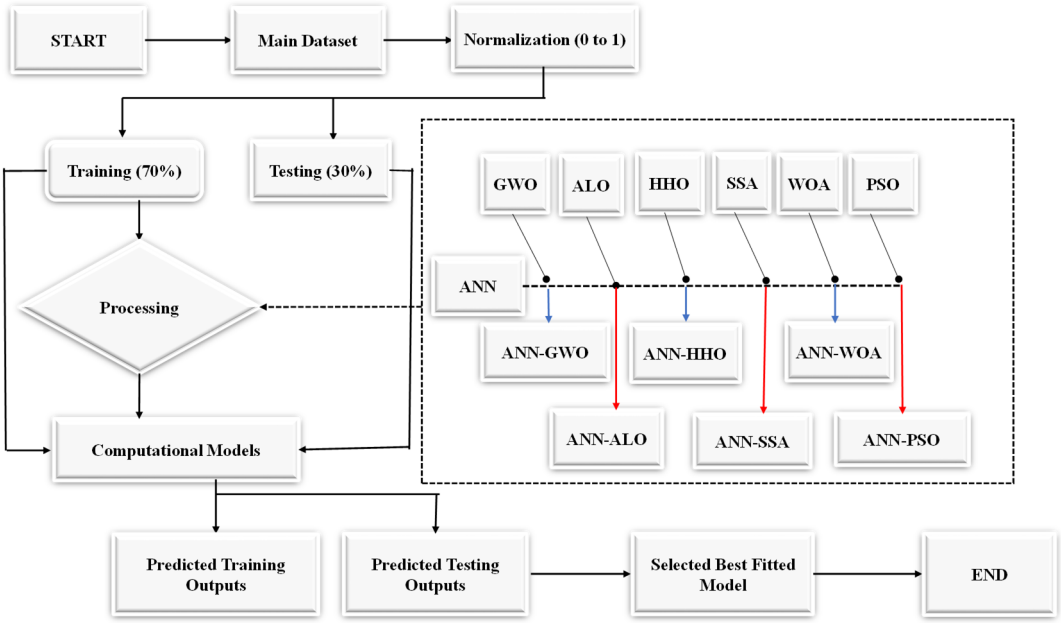

Figure 4. Flowchart of hybrid ANN models.

In this study, key hyperparameters (stated in Table 3) were selected through a structured and iterative tuning process guided by convergence behavior. Specifically, multiple combinations were evaluated within predefined ranges and the optimal configuration was selected based on minimum RMSE and consistent performance across training and testing datasets as shown in Table 3. The swarm size (NS) and number of iterations (Itr) were examined within practical ranges and values of 30 and 200, respectively, were found to provide stable convergence and computational efficiency hence these values were adopted for all hybrid ANN models to ensure a fair comparison. Figure 5 presents the convergence characteristics of the implemented algorithms demonstrating stable optimization behavior. The statistics indicate that ANN-ALO is the best convergent model followed by ANN-SSA. On the contrary, ANN-HHO followed by ANN-WOA performed poorly.

Table 3. Tuning of model hyperparameters.

Models	ANN-GWO	ANN-ALO	ANN-HHO	ANN-SSA	ANN-WOA	ANN-PSO
N_S	30	30	30	30	30	30
Itr	200	200	200	200	200	200
C	0.1064	0.21	11.56	73.22	98.325	0.05
γ	100	100	98.996	73.22	98.325	6.23

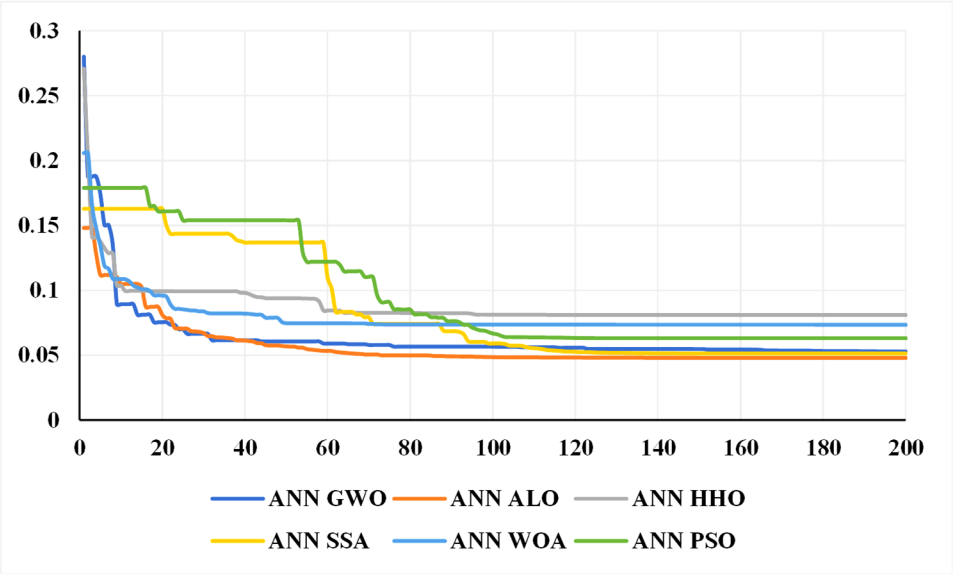

Figure 5. Convergence graph of the optimization algorithms.

3.2. Performance of Models

Table 4 shows the values of different performance indices for the proposed ANN based- hybrid models during the TR phase. It can be observed from Table 4 that ANN-ALO model performed better than the rest of the models by securing a higher R^2 = 0.9487 and a lower RMSE = 0.0478. Similarly, a very smaller value of WMAPE i.e., 0.1551 can be observed for the ANN-SSA model, in comparison to others. The second-best performing model is ANN-SSA having R^2 and RMSE values of 0.9408 and 0.0514. However, it is important to note here that ANN-ALO got the second lowest value of WMAPE i.e., 0.1561 after ANN-SSA (0.1551).

Similarly, Table 5 shows the values of different performance indices for the proposed ANN based- hybrid models during the TS phase. It can be observed from Table 5 that similar to its performance in the TR phase, the ANN-ALO model performed better again than the rest of the models by securing a higher R^2 = 0.9482 and a lower RMSE = 0.0539. Similarly, a very smaller value of 0.1753 of WMAPE can be observed for the ANN-ALO model, in comparison to others. The second-best performing model is ANN-SSA having R^2, RMSE and WMAPE values of 0.9347, 0.0588 and 0.1911. The ANN-GWO model improved its performance in the TS phase by securing a good value of R^2 = 0.9346, a lower RMSE of 0.0597 and second lowest value of MAE i.e., 0.0426 after ANN-ALO.

Table 6 presents the rankings of the proposed ANN-based hybrid models based on their R^2, RMSE, and MAE values in both the training and testing phases. As indicated in Tables 4–6, the ANN-ALO model demonstrated best performance across multiple evaluation metrics such as highest R^2 and the lowest RMSE and MAE in both phases. The ANN-SSA model ranked second overall, while the ANN-GWO model demonstrated competitive performance attaining the third-highest R^2 in both phases and the second-lowest MAE during testing.

Table 4. Performance of different ANN hybrid models during training phase.

Index	ANN-GWO	ANN-ALO	ANN-HHO	ANN-SSA	ANN-WOA	ANN-PSO
R^2	0.9374	0.9487	0.8555	0.9408	0.8825	0.9114
PI	1.8160	1.8446	1.6148	1.8245	1.6774	1.7502
VAF	93.74	94.87	85.40	94.08	87.94	91.04
RMSE	0.0528	0.0478	0.0809	0.0514	0.0733	0.0632
WI	0.9835	0.9867	0.9607	0.9845	0.9690	0.9768
MAE	0.0401	0.0380	0.0606	0.0378	0.0580	0.0488
RSR	0.2504	0.2266	0.3832	0.2434	0.3476	0.2994
WMAPE	0.1648	0.1561	0.2488	0.1551	0.2383	0.2005

Table 5. Performance of different ANN hybrid models during testing phase.

Index	ANN-GWO	ANN-ALO	ANN-HHO	ANN-SSA	ANN-WOA	ANN-PSO
R^2	0.9346	0.9482	0.8539	0.9347	0.8527	0.8939
PI	1.7919	1.8275	1.5765	1.7925	1.5789	1.6875
VAF	93.34	94.62	84.84	93.29	85.05	89.38
RMSE	0.0597	0.0539	0.0893	0.0588	0.0876	0.0737
WI	0.9824	0.9859	0.9597	0.9830	0.9606	0.9710
MAE	0.0426	0.0424	0.0703	0.0463	0.0655	0.0589
RSR	0.2641	0.2384	0.3948	0.2600	0.3872	0.3260
WMAPE	0.1759	0.1753	0.2903	0.1911	0.2707	0.2433

Table 6. Ranking of ANN based hybrid models based on different indices.

Statistic	R^2		RMSE		MAE	
Rank	1st	2nd	1st	2nd	1st	2nd
TR Phase	ANN-ALO	ANN-SSA	ANN-ALO	ANN-SSA	ANN-ALO	ANN-SSA
TS Phase	ANN-ALO	ANN-SSA	ANN-ALO	ANN-SSA	ANN-ALO	ANN-GWO

3.3. Visual Representation of Results

In addition to tabular presentation of results and their descriptive analysis, graphic depiction and representation of data has always been recommended and desired. The reason for their wide acceptance and requirement is that they allow easy spotting of trends and patterns in data and results. Keeping this in view, this study also made use of their benefit by visualizing the performance of the different proposed models using index scoring, accuracy matrix and Taylor diagram. It is important to recall here that accuracy matrix is a heat map which embodies the degree of accuracy and consistency of a prediction model using numerous performance indices.

Figure 6 presents the accuracy matrix of the proposed ANN-based hybrid models for both the training and testing phases. The matrix includes a color scale ranging from green (best performance) to red (poor performance). The results indicate that the ANN-ALO model outperformed the other models in both phases followed by ANN-SSA and ANN-GWO. In contrast, ANN-WOA and ANN-HHO exhibited comparatively lower performance in the training and testing phases, respectively as reflected from their R^2 and RMSE values.

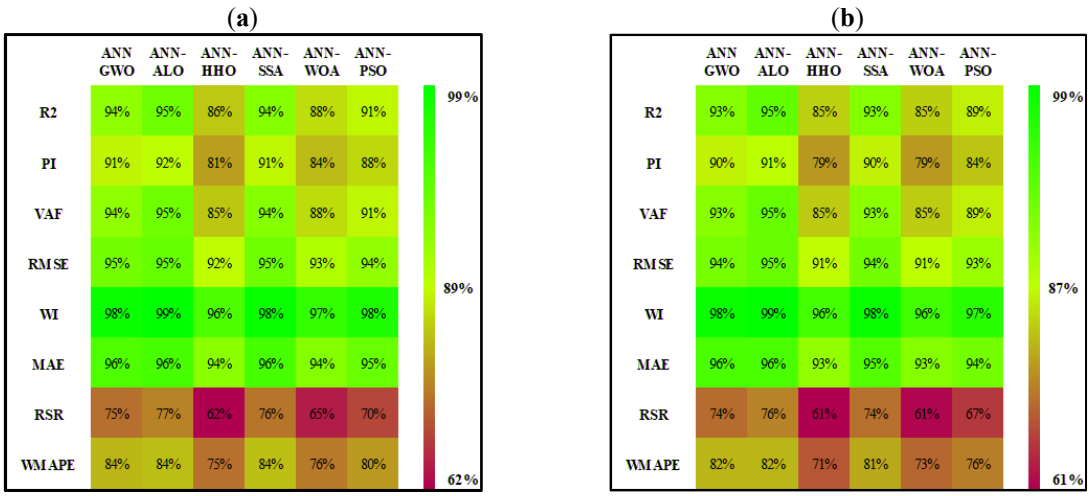

Figure 6. Accuracy matrix for the proposed hybrid ANN models during both TR and TS phase.

The Taylor diagram is a graphical tool used to compare model performance by illustrating the statistical relationship between predicted and reference (experimental) values. It is a two-dimensional representation based on three statistical measures: the correlation coefficient (R), RMSE, and the standard deviation ratio. Model performance is evaluated by plotting predicted values against the reference point enabling visual assessment of accuracy and agreement. Figure 7a,b present the Taylor diagrams for the proposed hybrid models during the training and testing phases, respectively. The ANN-ALO model exhibits the highest correlation coefficient (R > 0.94) in both phases. However, the standard deviation of ANN-SSA is closer to the reference value than that of ANN-ALO during the testing phase. These findings are consistent with the model rankings reported in Table 6. Additionally, the standard deviation values of ANN-HHO and ANN-WOA in the training phase and ANN-GWO and ANN-SSA in the testing phase are closer to the reference value than ANN-ALO as illustrated in Figure 7a,b.

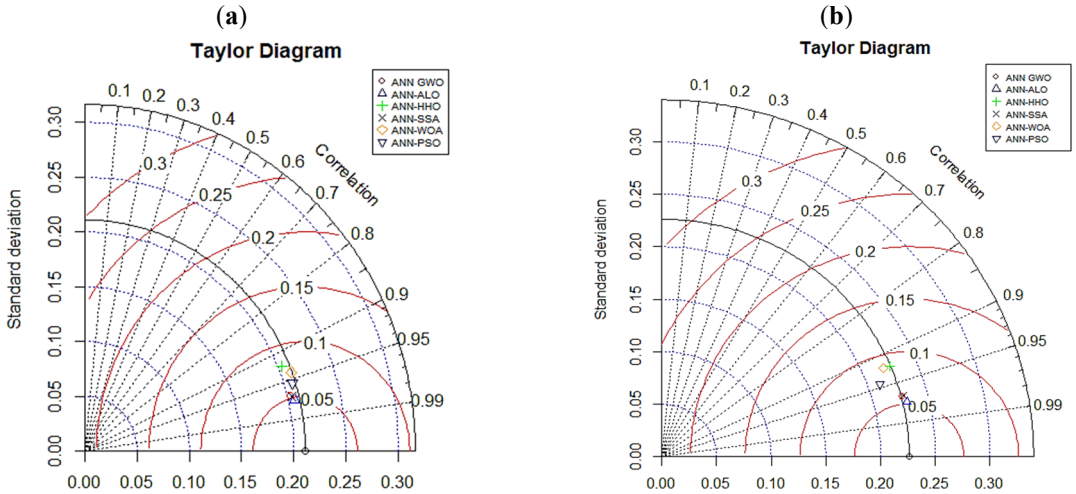

Figure 7. Taylor diagram for the proposed models; (**a**) Training phase and (**b**) Testing phase.

3.4. Comparison with ACI Equations

The ACI formulations based on the principles of mechanics are available to calculate the FS of FRP concrete beams. In order to avoid laborious calculation and uncertainties in material properties used in the mechanics-based equation, numerous researchers have worked on developing machine learning-based models to predict the flexural strength of FRP-reinforced beams [56]. The ACI guidelines are expressed in the form of mechanics based formulations as Equations (1)–(5). The predicted values from the most accurate model in this study were compared with previously developed GEP model [56] and the results obtained from the ACI equations. The results were reported in the form of P/E ratio. It is obvious from Figure 8a that significant proportion of the P/E ratios lies within ±10% for ACI formulations; however, for the GEP model developed in the previous study showed very less percentage of points within ±10% (Figure 8b). The results of ANN-ALO also showed comparable performance to ACI which interprets that the developed model in this study can be used reliably in predicting the new data (Figure 8c).

$$\rho_f = \frac{A_f}{bd} \tag{1}$$

A_f is the area of longitudinal flexural reinforcement (mm^2), ρ_f is FRP reinforcement ratio, d is the depth of the beam (mm) and b is width of the beam (mm).

$$\beta_1 = \begin{cases} 17 \le f_c' \le 28 & \beta_1 = 0.85 \\ 28 < f_c' < 55 & \beta_1 = 0.85 - \dfrac{0.05(f_c' - 28)}{7} \\ f_c' \ge 55 & \beta_1 = 0.65 \end{cases} \tag{2}$$

f_c' is the concrete compressive strength, β_1 is compressive stress block parameter.

When $\rho_f > \rho_b$

$$\boldsymbol{f_f} = \sqrt{\frac{(E_f \varepsilon_{cu})^2}{\mathbf{4}} + \frac{\mathbf{0.85}\beta_1 f_c'}{\rho_f} E_f \varepsilon_{cu}} - 0.5 E_f \varepsilon_{cu} \le f_{fu} \tag{3}$$

f_f is tensile stress of FRP rebar at failure, ρ_b is a balanced reinforcement ratio, ε_{cu} is ultimate concrete strain = 0.003, f_{fu} is ultimate tensile strength of FRP rebars, E_f is elastic modulus of longitudinal FRP bars

When $\rho_f < \rho_b$

$$c_b = \left(\frac{\varepsilon_{cu}}{\varepsilon_{cu} + \varepsilon_{fut}}\right) d \tag{4}$$

$$M_n = A_f f_{fu} \left(d - \frac{\beta_1 c_b}{2}\right) \tag{5}$$

c denotes the distance from the extreme compression fiber to the neutral axis of the member (mm), while c_b represents the corresponding distance at the balanced strain condition (mm).

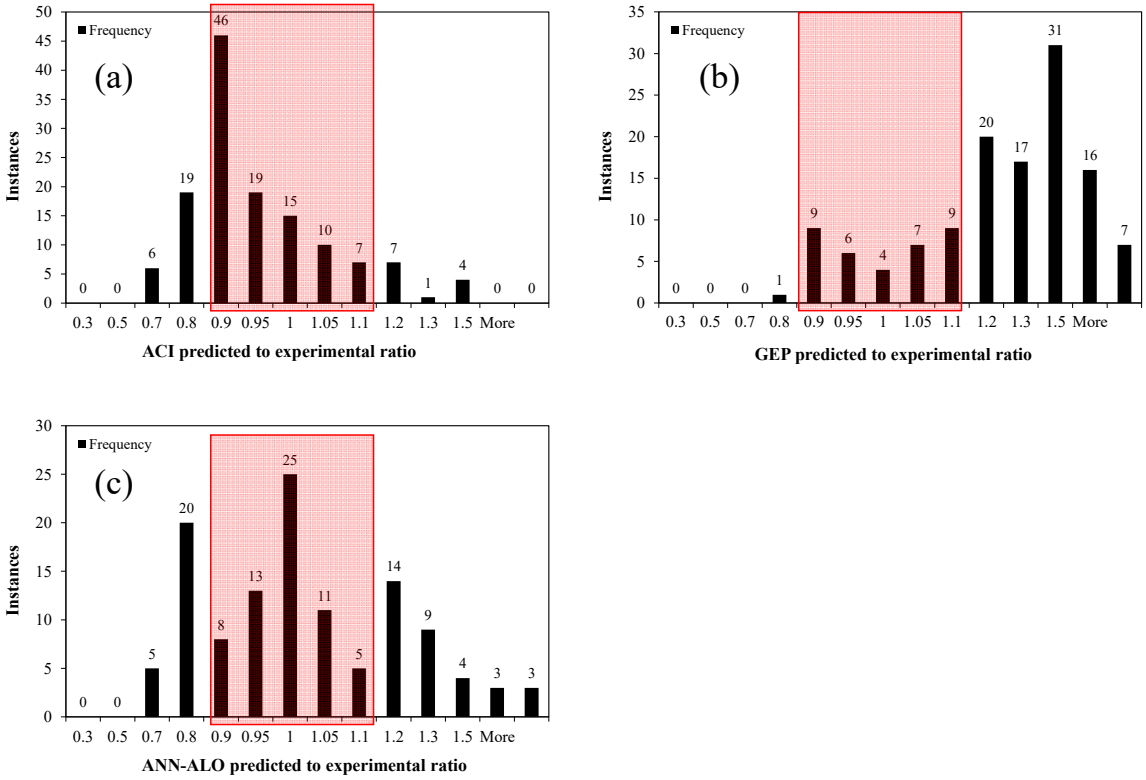

Figure 8. P/E ratio of different models (**a**) ACI, (**b**) GEP and (**c**) ANN-ALO.

However, it should be noted that the proposed ANN-based models are not intended to replace code-based design provisions but rather to serve as complementary tools for improved prediction, parametric evaluation and potential calibration of existing design guidelines.

4. Conclusions & Recommendations

This study proposed a novel comparative framework for six metaheuristic optimizers specifically tuned for the non-linear behavior of FRP-reinforced concrete beams by exploring their enhanced parameter optimization capability. For this purpose, experimental flexure strength values of FRP reinforced concrete beams was obtained from the published literature. Novel hybrid ANN based algorithms such as grey wolf optimizer, ant lion optimizer, Harris hawk optimizer, salp swarm, whale optimization and particle swarm optimization were trained and validated to predict the flexure strength of FRP reinforced concrete beams. Main conclusions drawn from this study are as follows:

1. ANN-ALO algorithm can be successfully applied to non-linear problems in the field of structural engineering due to its balanced approach between exploration and exploitation which enables better global search capability and avoidance of premature convergence. The excellent performance of the ANN-ALO model in predicting the flexure strength of FRP concrete beams as evidenced from its higher R^2 = 0.9487 and 0.9482 and a lower RMSE = 0.0478 and 0.0539 during the training and testing phases, respectively supports this conclusion.

2. Based on the values of R^2 and RMSE, ANN-SSA performed second to ANN-ALO due to its leader follower approach and an imbalance between exploration and exploitation. This increases the risk of stagnation and reduces diversity. Moreover, ANN-SSA gets trapped in local optima and converges too early.
3. Taylor diagrams revealed that the ANN-ALO model minimizes the global error as evident from its highest R value (>0.94 during training and testing phases, respectively) however, its standard deviation is lagging behind other hybrid algorithms due to overfitting and increased spread deviation. The standard deviation of ANN-SSA concludes its ability to preserve the statistical dispersion characteristics of the dataset and resulted in output variance more consistent with the experimental observations.
4. The comparison of the P/E ratios for the ANN-ALO predicted values, ACI codal formulations and previously published GEP model concluded that the ANN-ALO model yields more proximal results as majority of P/E ratios lies within ±10% of the experimental values while the GEP model showed strong deviations.

5. Limitations & Future Work

The performance of the developed hybrid ANN models is inherently dependent on the range and distribution of the experimental dataset used for training and testing, which may limit their extrapolation capability beyond the studied parameter space. Although model generalization was assessed using a training–testing split, more rigorous resampling techniques (e.g., k-fold cross-validation) were not implemented and could further quantify model stability and variance. The ANN-based framework operates as a data-driven, non-parametric model, and thus does not yield explicit closed-form equations comparable to conventional design formulations (e.g., ACI provisions).

Future studies should focus on expanding the experimental database to enhance the robustness and generalizability of hybrid ANN models. It can also be expanded to include 'Hybrid FRP' (e.g., Carbon + Glass) and its durability aspects which are critical for FRP-reinforced concrete. Additionally, the implementation of advanced validation strategies such as k-fold cross-validation, bootstrapping techniques, sensitivity analysis and statistical significance testing is recommended to further assess model stability and mitigate overfitting risks.

Author Contributions

M.I.: conceptualization, methodology, software, validation, writing—original draft preparation; M.R.: Methodology, data curation, investigation, validation, writing—original draft preparation, writing—review and editing. R.B.: Conceptualization, software, visualization, investigation, validation. All authors have read and agreed to the published version of the manuscript.

Funding

This research received no external funding.

Institutional Review Board Statement

Not applicable.

Informed Consent Statement

Not applicable.

Data Availability Statement

Dataset used for training and validation of machine learning models have been appended as Table A1.

Conflicts of Interest

The authors declare no conflict of interest. Given the role as Editorial Board Member, Mudassir Iqbal had no involvement in the peer review of this paper and had no access to information regarding its peer-review process. Full responsibility for the editorial process of this paper was delegated to another editor of the journal..

Use of AI and AI-Assisted Technologies

No AI tools were utilized for this paper.

Appendix A

Table A1. Dataset comprising inputs and output parameters used for training and validating the models.

b, mm	$f'c$, MPa	D, mm	A_s, mm^2	E_f, MPa	f_u, Mpa	Experimental Flexure Strength, MPa
200	240	35	508	43,370	885	39
200	240	36	508	43,370	885	41
130	180	57	238	38,000	773	20
130	180	97	238	38,000	773	23
130	180	46	475	38,000	773	21
130	180	54	475	38,000	773	21
130	180	94	475	38,000	773	28
180	300	35	253	40,000	695	59
180	300	35	380	40,000	695	65
180	300	35	380	40,000	695	64
180	300	35	507	40,000	695	71
200	300	40	284	114,000	1506	71
200	300	39	425	114,000	1506	83
200	300	41	382	122,000	1988	81
200	300	41	509	122,000	1988	89
200	300	39	760	40,000	617	77
200	300	39	679	36,000	747	71
200	300	39	905	36,000	747	85
200	300	39	425	52,000	1800	71
200	300	39	567	52,000	1800	72
200	450	52	573	49,000	641	107
200	450	52	573	49,000	641	113
200	550	43	573	42,000	689	182
200	550	43	573	49,000	641	147
150	200	28	57	38,000	650	6
150	250	28	57	38,000	650	8
150	200	50	57	38,000	650	6
150	250	50	57	38,000	650	9
150	300	50	113	38,000	650	17
200	300	43	573	45,000	600	80
381	203	28	80	41,400	830	11
381	203	28	80	41,400	830	13
381	203	28	80	41,400	830	11
318	216	28	80	41,400	830	14
318	216	28	80	41,400	830	13
318	216	28	80	41,400	830	13
203	152	28	320	41,400	830	16
203	152	28	320	41,400	830	16
203	152	28	320	41,400	830	16
191	152	28	320	41,400	830	17
191	152	28	320	41,400	830	16
200	300	52	349	37,600	773	58
200	300	52	349	37,600	773	60
200	300	52	523	37,600	773	66
200	300	52	523	37,600	773	65
200	300	45	1046	37,600	773	85
152	152	36	71	44,800	760	7
152	152	36	71	44,800	760	7
152	152	36	71	44,800	760	7
152	152	36	71	44,800	760	7
150	250	32	429	45,000	1000	40
200	210	31	1134	35,630	700	34
200	260	31	507	43,370	886	45
200	300	24	88	200,000	2000	45
200	300	27	226	200,000	1061	61
152	152	49	99	140,000	1900	17
200	400	34	261	67,000	1639	83
200	400	34	385	48,700	817	81

Table A1. *Cont.*

b, mm	*f'c*, MPa	*D*, mm	A_s, mm^2	E_f, MPa	f_u, Mpa	Experimental Flexure Strength, MPa
200	400	29	970	69,300	1362	129
200	400	34	1162	50,000	762	119
200	400	73	970	69,300	1362	178
200	400	34	970	59,500	1245	111
200	400	73	1040	59,500	1245	188
200	400	73	1019	60,300	906	189
152	305	29	1013	45,500	552	54
152	305	34	774	50,600	552	56
152	305	45	1006	45,500	552	74
152	305	45	1006	45,500	552	81
152	305	45	381	48,300	738	42
152	305	45	355	47,700	896	51
178	229	48	723	41,000	690	47
178	229	48	1077	41,000	552	51
178	229	48	219	124,000	2069	51
280	380	37	804	40,000	593	159
280	380	41	1964	38,000	582	238
280	380	42	339	40,200	603	80
200	294	54	299	45,000	552	41
200	294	43	299	49,000	641	53
200	294	43	449	49,000	641	62
230	256	40	603	50,000	1000	54
180	165	30	115	42,900	1121	21
180	165	30	115	42,900	1121	22
180	165	30	243	46,600	1118	29
180	165	30	365	46,600	1118	36
180	165	30	424	46,000	1075	38
180	165	30	424	46,000	1075	41
180	165	47	172	42,900	1075	23
180	165	47	171	42,800	1029	23
180	165	47	243	46,600	1119	31
180	165	47	636	46,000	1121	38
180	165	70	171	42,800	1029	25
180	165	70	243	46,600	1119	32
180	165	70	636	46,000	1121	45
180	165	70	243	130,000	2068	50
200	240	36	508	43,370	885	39
130	180	57	238	38,000	773	21
180	300	35	253	40,000	695	60
200	300	40	254	122,000	1988	79
200	300	39	1013	40,000	617	87
200	300	44	573	42,000	689	80
200	300	44	573	49,000	641	51
200	300	44	573	49,000	641	64
200	550	43	573	49,000	641	173
200	550	43	573	45,000	600	182
200	300	45	1046	37,600	773	85
150	250	32	429	45,000	1000	40
200	300	41	567	35,630	700	59
200	250	41	1134	35,630	700	57
200	400	59	385	48,700	817	86
280	380	43	452	40,200	603	107
200	294	43	299	45,000	552	39
230	254	40	339	50,000	1000	53
180	165	47	243	130,000	2068	41
180	165	70	172	42,900	1075	26
200	240	35	508	43,370	885	41
130	180	54	475	38,000	773	21
130	180	94	475	38,000	773	30
180	300	35	507	40,000	695	71

Table A1. *Cont.*

b, mm	*f'c*, MPa	*D*, mm	A_s, mm^2	E_f, MPa	f_u, Mpa	Experimental Flexure Strength, MPa
200	300	39	567	114,000	1506	90
200	550	43	573	42,000	689	182
150	300	28	57	38,000	650	11
200	550	43	573	45,000	600	182
191	152	28	320	41,400	830	16
200	300	45	697	37,600	773	75
200	300	45	697	37,600	773	72
152	152	36	71	44,800	760	7
150	250	25	429	45,000	1000	40
152	152	52	63	140,000	1900	13
200	400	59	261	67,000	1639	102
200	400	73	1162	50,000	762	178
200	400	34	1019	60,300	906	116
280	380	34	1964	38,000	582	237
200	270	42	1356	38,000	773	85
230	254	40	226	50,000	1000	49

References

1. Szostak, B.; Golewski, G.L. Improvement of strength parameters of cement matrix with the addition of siliceous fly ash by using nanometric C-S-H seeds. *Energies* **2020**, *13*, 6734. https://doi.org/10.3390/en13246734.
2. Grzymski, F.; Musiał, M.; Trapko, T. Mechanical properties of fibre reinforced concrete with recycled fibres. *Constr. Build. Mater.* **2019**, *198*, 323–331. https://doi.org/10.1016/j.conbuildmat.2018.11.183.
3. Neville, A.M. *Properties of Concrete*, 5th ed.; Prentice Hall: Hoboken, NJ, USA, 1963.
4. Rashad, A.M. A brief on high-volume Class F fly ash as cement replacement—A guide for Civil Engineer. *Int. J. Sustain. Built Environ.* **2015**, *4*, 278–306. https://doi.org/10.1016/j.ijsbe.2015.10.002.
5. Bai, Y.; Nardi, D.C.; Zhou, X.; et al. A new comprehensive model of damage for flexural subassemblies prone to fatigue. *Comput. Struct.* **2021**, *256*, 106639. https://doi.org/10.1016/j.compstruc.2021.106639.
6. Lee, W.T.; Chiou, Y.J.; Shih, M.H. Reinforced concrete beam-column joint strengthened with carbon fiber reinforced polymer. *Compos. Struct.* **2010**, *92*, 48–60. https://doi.org/10.1016/j.compstruct.2009.06.011.
7. Golewski, G.L.; Gil, D.M. Studies of fracture toughness in concretes containing fly ash and silica fume in the first 28 days of curing. *Materials* **2021**, *14*, 319. https://doi.org/10.3390/ma14020319.
8. Li, B.; Chi, Y.; Xu, L.; et al. Experimental investigation on the flexural behavior of steel-polypropylene hybrid fiber reinforced concrete. *Constr. Build. Mater.* **2018**, *191*, 80–94. https://doi.org/10.1016/j.conbuildmat.2018.09.202.
9. Zhou, X.; et al. Damage Evolution Modeling for Steel Structures Subjected to Combined High Cycle Fatigue and High-Intensity Dynamic Loadings. *Int. J. Struct. Stab. Dyn.* **2022**, *22*, 2240012. https://doi.org/10.1142/S0219455422400120.
10. Liu, Y.; Zhang, Z.; Liu, X.; et al. Efficient image segmentation based on deep learning for mineral image classification. *Adv. Powder Technol.* **2021**, *32*, 3885–3903. https://doi.org/10.1016/j.apt.2021.08.038.
11. Guo, R.; Xian, G.; Li, F.; et al. Hygrothermal resistance of pultruded carbon, glass and carbon/glass hybrid fiber reinforced epoxy composites. *Constr. Build. Mater.* **2022**, *315*, 125710. https://doi.org/10.1016/j.conbuildmat.2021.125710.
12. Robert, M.; Benmokrane, B. Combined effects of saline solution and moist concrete on long-term durability of GFRP reinforcing bars. *Constr. Build. Mater.* **2013**, *38*, 274–284. https://doi.org/10.1016/j.conbuildmat.2012.08.021.
13. Wang, Z.; et al. Long-term durability of basalt- and glass-fibre reinforced polymer (BFRP/GFRP) bars in seawater and sea sand concrete environment. *Constr. Build. Mater.* **2017**, *139*, 467–489. https://doi.org/10.1016/j.conbuildmat.2017.02.038.
14. Huang, H.; Huang, M.; Zhang, W.; et al. Experimental Investigation on Rehabilitation of Corroded RC Columns with BSP and HPFL under Combined Loadings. *J. Struct. Eng.* **2020**, *146*, 04020123. https://doi.org/10.1061/(asce)st.1943-541x.0002725.
15. Rodrigues, R.; Gaboreau, S.; Gance, J.; et al. Reinforced concrete structures: A review of corrosion mechanisms and advances in electrical methods for corrosion monitoring. *Constr. Build. Mater.* **2021**, *269*, 121240. https://doi.org/10.1016/j.conbuildmat.2020.121240.
16. Polder, R.B.; Peelen, W.H.A.; Courage, W.M.G. Non-traditional assessment and maintenance methods for aging concrete structures—Technical and non-technical issues. *Mater. Corros.* **2012**, *63*, 1147–1153. https://doi.org/10.1002/maco.201206725.
17. Huang, H.; Huang, M.; Zhang, W.; Yang, S. Experimental study of predamaged columns strengthened by HPFL and BSP under combined load cases. *Struct. Infrastruct. Eng.* **2021**, *17*, 1210–1227. https://doi.org/10.1080/15732479.2020.1801768.
18. Lan, M.Y.; Zheng, M.B.; Shi, T.; et al. Crack resistance property of carbon nanotubes-modified concrete. *Mag. Concr. Res.* **2022**, *74*, 1133–1145. https://doi.org/10.1680/jmacr.21.00227.

19. Gedik, A. A review on the evaluation of the potential utilization of construction and demolition waste in hot mix asphalt pavements. *Resour. Conserv. Recycl.* **2020**, *161*, 104956. https://doi.org/10.1016/j.resconrec.2020.104956.
20. Saiu, V.; Blečić, I.; Meloni, I. Making sustainability development goals (SDGs) operational at suburban level: Potentials and limitations of neighbourhood sustainability assessment tools. *Environ. Impact Assess. Rev.* **2022**, *96*, 106845. https://doi.org/10.1016/j.eiar.2022.106845.
21. Yang, J.; Haghani, R.; Blanksvärd, T.; Lundgren, K. Experimental study of FRP-strengthened concrete beams with corroded reinforcement. *Constr. Build. Mater.* **2021**, *301*, 124076. https://doi.org/10.1016/j.conbuildmat.2021.124076.
22. Angst, U.M. Challenges and opportunities in corrosion of steel in concrete. *Mater. Struct.* **2018**, *51*, 4. https://doi.org/10.1617/s11527-017-1131-6.
23. Wei, J.; Xie, Z.; Zhang, W.; et al. Experimental study on circular steel tube-confined reinforced UHPC columns under axial loading. *Eng. Struct.* **2021**, *230*, 111599. https://doi.org/10.1016/j.engstruct.2020.111599.
24. Wang, X.; Yang, Y.; Yang, R.; Liu, P. Experimental Analysis of Bearing Capacity of Basalt Fiber Reinforced Concrete Short Columns under Axial Compression. *Coatings* **2022**, *12*, 654. https://doi.org/10.3390/coatings12050654.
25. Zhu, Z.; Wu, Y.; Liang, Z. Mining-Induced Stress and Ground Pressure Behavior Characteristics in Mining a Thick Coal Seam With Hard Roofs. *Front. Earth Sci.* **2022**, *10*, 843191. https://doi.org/10.3389/feart.2022.843191.
26. Al-Jaberi, Z.; Myers, J.J.; Chandrashekhara, K. Effect of direct service temperature exposure on the bond behavior between advanced composites and CMU using NSM and EB techniques. *Compos. Struct.* **2019**, *211*, 63–75. https://doi.org/10.1016/j.compstruct.2018.11.085.
27. Ahmed, A.; Guo, S.; Zhang, Z.; et al. A review on durability of fiber reinforced polymer (FRP) bars reinforced seawater sea sand concrete. *Constr. Build. Mater.* **2020**, *256*, 119484. https://doi.org/10.1016/j.conbuildmat.2020.119484.
28. Bakay, R.; Shrive, N.G.; Sayed-Ahmed, E.Y. Bond Strength of FRP Laminates to Concrete: State-of-the-Art Review. *Electron. J. Struct. Eng.* **2009**, *9*, 45–61.
29. Zhang, C.; Ali, A.; Sun, L. Investigation on low-cost friction-based isolation systems for masonry building structures: Experimental and numerical studies. *Eng. Struct.* **2021**, *243*, 112645. https://doi.org/10.1016/j.engstruct.2021.112645.
30. Cheng, H.; Sun, L.; Wang, Y.; Chen, X. Effects of actual loading waveforms on the fatigue behaviours of asphalt mixtures. *Int. J. Fatigue* **2021**, *151*, 106386. https://doi.org/10.1016/j.ijfatigue.2021.106386.
31. Shi, T.; et al. Calcined Attapulgite Clay as Supplementary Cementing Material: Thermal Treatment, Hydration Activity and Mechanical Properties. *Int. J. Concr. Struct. Mater.* **2022**, *16*, 25. https://doi.org/10.1186/s40069-022-00499-8.
32. Zhou, J.; Chen, X.; Chen, S. Durability and service life prediction of GFRP bars embedded in concrete under acid environment. *Nucl. Eng. Des.* **2011**, *241*, 4095–4102. https://doi.org/10.1016/j.nucengdes.2011.08.038.
33. Wang, L.; Mao, Y.; Lv, H.; et al. Bond properties between FRP bars and coral concrete under seawater conditions at 30, 60, and 80 °C. *Constr. Build. Mater.* **2018**, *162*, 442–449. https://doi.org/10.1016/j.conbuildmat.2017.12.058.
34. Li, S.; Guo, S.; Yao, Y.; et al. The effects of aging in seawater and SWSSC and strain rate on the tensile performance of GFRP/BFRP composites: A critical review. *Constr. Build. Mater.* **2021**, *282*, 122534. https://doi.org/10.1016/j.conbuildmat.2021.122534.
35. Chen, Y.; Davalos, J.F.; Ray, I.; Kim, H.Y. Accelerated aging tests for evaluations of durability performance of FRP reinforcing bars for concrete structures. *Compos. Struct.* **2007**, *78*, 101–111. https://doi.org/10.1016/j.compstruct.2005.08.015.
36. Liu, Y.; Zhang, Z.; Liu, X.; et al. Ore image classification based on small deep learning model: Evaluation and optimization of model depth, model structure and data size. *Miner. Eng.* **2021**, *172*, 107020. https://doi.org/10.1016/j.mineng.2021.107020.
37. Armaghani, D.J.; Asteris, P.G. A comparative study of ANN and ANFIS models for the prediction of cement-based mortar materials compressive strength. *Neural Comput. Appl.* **2021**, *33*, 4501–4516. https://doi.org/10.1007/s00521-020-05244-4.
38. Heidari, M.R.; Heravi, G.; Esmaeeli, A.N. Integrating life-cycle assessment and life-cycle cost analysis to select sustainable pavement: A probabilistic model using managerial flexibilities. *J. Clean. Prod.* **2020**, *254*, 120046. https://doi.org/10.1016/j.jclepro.2020.120046.
39. Shahmansouri, A.A.; Akbarzadeh Bengar, H.; Ghanbari, S. Compressive strength prediction of eco-efficient GGBS-based geopolymer concrete using GEP method. *J. Build. Eng.* **2020**, *31*, 101326. https://doi.org/10.1016/j.jobe.2020.101326.
40. Zhou, J.; Li, C.; Arslan, C.A.; et al. Performance evaluation of hybrid FFA-ANFIS and GA-ANFIS models to predict particle size distribution of a muck-pile after blasting. *Eng. Comput.* **2021**, *37*, 265–274. https://doi.org/10.1007/s00366-019-00822-0.
41. Wu, Z.; Xu, J.; Li, Y.; Wang, S. Disturbed State Concept–Based Model for the Uniaxial Strain-Softening Behavior of Fiber-Reinforced Soil. *Int. J. Geomech.* **2022**, *22*, 04022092. https://doi.org/10.1061/(asce)gm.1943-5622.0002415.
42. Hao, R.B.; Lu, Z.Q.; Ding, H.; Chen, L.Q. A nonlinear vibration isolator supported on a flexible plate: Analysis and experiment. *Nonlinear Dyn.* **2022**, *108*, 941–958. https://doi.org/10.1007/s11071-022-07243-7.

43. Sarker, I.H. Deep Learning: A Comprehensive Overview on Techniques, Taxonomy, Applications and Research Directions. *SN Comput. Sci.* **2021**, *2*, 420. https://doi.org/10.1007/s42979-021-00815-1.
44. Jiang, H.; Mohammed, A.S.; Kazeroon, R.A.; Sarir, P. Use of the Gene-Expression Programming Equation and FEM for the High-Strength CFST Columns. *Appl. Sci.* **2021**, *11*, 10468. https://doi.org/10.3390/app112110468.
45. Perveen, G.; Rizwan, M.; Goel, N. An ANFIS-based model for solar energy forecasting and its smart grid application. *Eng. Rep.* **2019**, *1*, e12070. https://doi.org/10.1002/eng2.12070.
46. Xu, J.; Wu, Z.; Chen, H.; et al. Influence of dry-wet cycles on the strength behavior of basalt-fiber reinforced loess. *Eng. Geol.* **2022**, *302*, 106645. https://doi.org/10.1016/j.enggeo.2022.106645.
47. Hu, Z.; et al. Research progress on lunar and Martian concrete. *Constr. Build. Mater.* **2022**, *343*, 128117. https://doi.org/10.1016/j.conbuildmat.2022.128117.
48. Guo, Y.; Yang, Y.; Kong, Z.; He, J. Development of Similar Materials for Liquid-Solid Coupling and Its Application in Water Outburst and Mud Outburst Model Test of Deep Tunnel. *Geofluids* **2022**, *2022*, 8784398. https://doi.org/10.1155/2022/8784398.
49. Baykasoğlu, A.; Öztaş, A.; Özbay, E. Prediction and multi-objective optimization of high-strength concrete parameters via soft computing approaches. *Expert Syst. Appl.* **2009**, *36*, 6145–6155. https://doi.org/10.1016/j.eswa.2008.07.017.
50. Topçu, I.B.; Saridemir, M. Prediction of compressive strength of concrete containing fly ash using artificial neural networks and fuzzy logic. *Comput. Mater. Sci.* **2008**, *41*, 305–311. https://doi.org/10.1016/j.commatsci.2007.04.009.
51. Saridemir, M. Predicting the compressive strength of mortars containing metakaolin by artificial neural networks and fuzzy logic. *Adv. Eng. Softw.* **2009**, *40*, 920–927. https://doi.org/10.1016/j.advengsoft.2008.12.008.
52. Dahish, H.A.; Alkharisi, M.K.; Abouelnour, M.A.; et al. Predicting the Compressive Strength of Waste Powder Concrete Using Response Surface Methodology and Neural Network Algorithm. *Buildings* **2025**, *15*, 3934. https://doi.org/10.3390/buildings15213934.
53. Mohammadi Golafshani, E.; Arashpour, M.; Behnood, A. Predicting the compressive strength of green concretes using Harris hawks optimization-based data-driven methods. *Constr. Build. Mater.* **2022**, *318*, 125944. https://doi.org/10.1016/j.conbuildmat.2021.125944.
54. Khan, K.; Salami, B.A.; Iqbal, M.; et al. Compressive Strength Estimation of Fly Ash/Slag Based Green Concrete by Deploying Artificial Intelligence Models. *Materials* **2022**, *15*, 3722. https://doi.org/10.3390/ma15103722.
55. Shariati, M.; et al. A novel hybrid extreme learning machine–grey wolf optimizer (ELM-GWO) model to predict compressive strength of concrete with partial replacements for cement. *Eng. Comput.* **2022**, *38*, 757–779. https://doi.org/10.1007/s00366-020-01081-0.
56. Murad, Y.; et al. Flexural strength prediction for concrete beams reinforced with FRP bars using gene expression programming. *Structures* **2021**, *33*, 3163–3172. https://doi.org/10.1016/j.istruc.2021.06.045.
57. Marani, A.; Nehdi, M.L. Predicting shear strength of FRP-reinforced concrete beams using novel synthetic data driven deep learning. *Eng. Struct.* **2022**, *257*, 114083. https://doi.org/10.1016/j.engstruct.2022.114083.
58. Fathy, I.N.; Dahish, H.A.; Alkharisi, M.K.; et al. Predicting the compressive strength of concrete incorporating waste powders exposed to elevated temperatures utilizing machine learning. *Sci. Rep.* **2025**, *15*, 25275. https://doi.org/10.1038/s41598-025-11239-9.
59. Naderpour, H.; Nagai, K.; Fakharian, P.; Haji, M. Innovative models for prediction of compressive strength of FRP-confined circular reinforced concrete columns using soft computing methods. *Compos. Struct.* **2019**, *215*, 69–84. https://doi.org/10.1016/j.compstruct.2019.02.048.
60. Song, H.; et al. Predicting the compressive strength of concrete with fly ash admixture using machine learning algorithms. *Constr. Build. Mater.* **2021**, *308*, 125021. https://doi.org/10.1016/j.conbuildmat.2021.125021.
61. Mirjalili, S.; Mirjalili, S.M.; Lewis, A. Grey Wolf Optimizer. *Adv. Eng. Softw.* **2014**, *69*, 46–61. https://doi.org/10.1016/j.advengsoft.2013.12.007.
62. Mirjalili, S. The Ant Lion Optimizer. *Adv. Eng. Softw.* **2015**, *83*, 80–98. https://doi.org/10.1016/j.advengsoft.2015.01.010.
63. Heidari, A.A.; Mirjalili, S.; Faris, H.; et al. Harris hawks optimization: Algorithm and applications. *Future Gener. Comput. Syst.* **2019**, *97*, 849–872. https://doi.org/10.1016/j.future.2019.02.028.
64. Mirjalili, S.; Gandomi, A.H.; Mirjalili, S.Z.; et al. Salp Swarm Algorithm: A bio-inspired optimizer for engineering design problems. *Adv. Eng. Softw.* **2017**, *114*, 163–191. https://doi.org/10.1016/j.advengsoft.2017.07.002.
65. Zhu, Z.; Wu, Y.; Han, J. A Prediction Method of Coal Burst Based on Analytic Hierarchy Process and Fuzzy Comprehensive Evaluation. *Front. Earth Sci.* **2022**, *9*, 834958. https://doi.org/10.3389/feart.2021.834958.
66. Mirjalili, S.; Lewis, A. The Whale Optimization Algorithm. *Adv. Eng. Softw.* **2016**, *95*, 51–67. https://doi.org/10.1016/j.advengsoft.2016.01.008.
67. Eberhart, R.C.; Kennedy, J. Particle swarm optimization. In Proceedings of ICNN'95—International Conference on Neural Networks, Perth, WA, Australia, 27 November–1 December 1995; Volume 4, pp. 1942–1948. https://doi.org/10.1109/ICNN.1995.488968.

68. Mohammadzadeh, D.; Bolouri Bazaz, J.; Alavi, A.H. An evolutionary computational approach for formulation of compression index of fine-grained soils. *Eng. Appl. Artif. Intell.* **2014**, *33*, 58–68. https://doi.org/10.1016/j.engappai.2014.03.012.
69. Bardhan, A.; et al. A novel integrated approach of augmented grey wolf optimizer and ANN for estimating axial load carrying-capacity of concrete-filled steel tube columns. *Constr. Build. Mater.* **2022**, *337*, 127454. https://doi.org/10.1016/j.conbuildmat.2022.127454.